第 27 卷第 6 期 无 机 化 学 学 报 Vol.27 No.6
2011 年 6 月 CHINESE JOURNAL OF INORGANIC CHEMISTRY 1202-1206

煤炭燃烧过程中 N_2O 消除反应机理的密度泛函理论研究

周素芹* 谷亚昕 固 旭
(江苏省凹土资源利用重点实验室,江苏淮阴工学院,生命科学与化学工程学院,淮安 223003)

摘要:用密度泛函理论 B3LYP 方法对煤炭燃烧过程中 N_2O 的消除反应进行研究。选用 6-311++G** 和 aug-cc-pVTZ 基组,优化了反应通道上反应物、过渡态和产物的几何构型。预测了它们的热力学性质(总能量、焓、熵和吉布斯自由能)及其随温度的变化。预测 N_2O+CO 反应的活化能为 200 kJ·mol^{-1},与实验值 193±8 kJ·mol^{-1} 较一致。计算了 500~1 800 K 温度范围的反应速率常数。在 N_2O 的分解中,N_2O 与 H 和 CN 自由基的反应为动力学优先进行的反应,其活化能为 50~55 kJ·mol^{-1}。在 B3LYP/aug-cc-pVTZ level 水平下,N_2O+CN 反应是热力学最有利的自发反应,其吉布斯自由能变化为–407 kJ·mol^{-1}。

关键词:N_2O 消除反应; 煤炭燃烧; 反应机理; 密度泛函理论; 过渡态
中图分类号:O613.61 **文献标识码**:A **文章编号**:1001-4861(2011)06-1202-05

Mechanism of N_2O Destruction under Coal Combustion Conditions: Density Functional Theory Study

ZHOU Su-Qin* GU Ya-Xin GU Xu
(*Key Laboratory for Attapulgite Science and Applied Technology of Jiangsu Province, College of Life Science and Chemical Engineering, Huaiyin Institute of Technology, Huaian, Jiangsu* 223003, *China*)

Abstract: We have calculated the reactants, transition states and products of six reactions involving the N_2O destruction under coal combustion, by using the DFT-B3LYP method with the 6-311++G** and aug-cc-pVTZ basis sets. Optimized structures were obtained. Thermodynamic property changes (total energy, enthalpy, entropy and Gibbs free energy) along the reaction paths, as well as their variations with temperatures, were predicted. The predicted activation energy of *ca.* 200 kJ·mol^{-1} for the reaction of N_2O+CO is in good agreement with experiment value of 193±8 kJ·mol^{-1}. Rate constants over the temperature range of 500~1 800 K were figured out. The reactions of N_2O with H and CN radicals are kinetically the leading roles in N_2O destruction, with activation energies of 50~55 kJ·mol^{-1}. The reaction of N_2O with CN radical is thermodynamically the most favorable process with Gibbs free energy changes of –407 kJ·mol^{-1} at the B3LYP/aug-cc-pVTZ level.

Key words: nitrous oxygen destruction; coal combustion; mechanism; density functional theory; transition state

0 Introduction

Increasing awareness about the environmental problems related to NO_x emissions from coal combustion has led the researchers to lay more emphasis on the combustion chemistry and chemical kinetics of NO_x. Nitrous oxide has become the subject of intense research and debate because of its increasing concentrations in the atmosphere and its known ability to deplete the ozone layer and also to contribute to the greenhouse effect[1-7]. The global warming potential of N_2O is about 300 times as effective as CO_2 for per unit mass[8]. It is

收稿日期:2010-11-01。收修改稿日期:2011-01-11。
江苏省自然科学基金(No.BK2008195)和淮安市工业支撑计划(No.HAG09011)资助项目。
*通讯联系人。E-mail:zhousuqin7803@sina.com

agreed that N_2O levels in the atmosphere are increasing at around 0.2 percent per year. At the current rate of production, it is estimated that N_2O concentrations will reach roughly 3.75×10^{-7} by the year 2030[5]. Besides, N_2O has an average residence time in the atmosphere of 170 years. Thus, N_2O is stable enough to rise through the atmosphere and reach the ozone layer in the stratosphere, where it is photochemically oxidized to nitric oxide (NO). Nitric oxide then attacks ozone and changes it into oxygen. Thus, the stability of N_2O makes its direct effect on the ozone layer larger than that of NO, whose high reactivity ensures its consumption before NO can reach the stratosphere[5]. There were some experimental and theoretical investigations for the N_2O destruction reactions. It was found that the N_2O destruction rates in the presence of CO were increased hundreds to thousands times higher than those in the absence of CO over the mixed transition metal oxide catalysts[9]. Kimberly et al. performed a quasiclassical trajectory study of $H+N_2O$ reaction, and found that the higher energies directed reaction via O-atom attack dominates[10]. Loriat el al made kinetic measurements on the oxidation of carbon monoxide by nitrous oxide between 1 076 and 1 228 K and obtained the rate constant of the exchange reaction[8]. Theoretical investigation for the reaction of N_2O with CO catalyzed by some metal cations and its oxides has also received more and more attention[11-12].

The reactions of N_2O destruction are very complicated. We focus here only on the direct pathway. In this work we have applied DFT methods for the evaluation of the mechanisms of the reactions:

$$N_2O+H \longrightarrow N_2+OH \quad (1)$$

$$N_2O+OH \longrightarrow N_2+HO_2 \quad (2)$$

$$N_2O+O(3P) \longrightarrow N_2+O_2 \quad (3)$$

$$N_2O+O(3P) \longrightarrow NO+NO \quad (4)$$

$$N_2O+CO \longrightarrow N_2+CO_2 \quad (5)$$

$$N_2O+CN \longrightarrow NCO+N_2 \quad (6)$$

These reactions are of great interest in combustion chemistry as well as in atmospheric chemistry. The main goal is to explore the pathway of the above N_2O destruction reactions, the activation energies, and the rate constants.

1 Experimental

Computational methods: The DFT-B3LYP[13-15] with both 6-311++G** and aug-cc-pVTZ basis sets was used for the location of transition states (TS). Computations were also performed with the Gaussian 03 package[16]. The optimizations were performed without any symmetry restrictions using the default convergence criteria in the programs. All of the optimized structures of reactants and products were characterized to be true local energy minima on the potential energy surfaces without imaginary frequencies. While the optimized structures of transition states were verified by only one imaginary frequency and intrinsic reaction coordinate (IRC) calculation with a reaction path being followed.

2 Results and discussions

2.1 Optimized geometries

Fig.1 shows the optimized structures of reactants and products. Fig.2 displays the structures of transition states. All the energies were corrected for the zero-point vibrational energy (ZPE) with scaling factors of 0.96[17]. The optimized geometrical parameters at the B3LYP/6-311++G** and B3LYP/aug-cc-pVTZ levels are nearly the same. Bond lengths at the former level are equal to or slightly larger than those at the latter level, with the exception of O-O distance in TS2. Since the optimized geometries from the two computational levels are almost identical, we discuss the geometrical changes along the reaction paths, as well as the thermodynamic property changes thereafter, at the B3LYP/aug-cc-pVTZ level. For reactants and products, species having three atoms are linear with exception of O_2H. However, the linearity

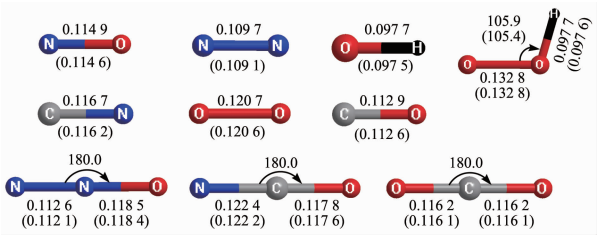

Data in parenthesis belong to the latter, bond length in nm and bond angle in (°)

Fig.1 Molecular structures of reactants and products at the B3LYP/6-311++G** and B3LYP/aug-cc-pVTZ levels

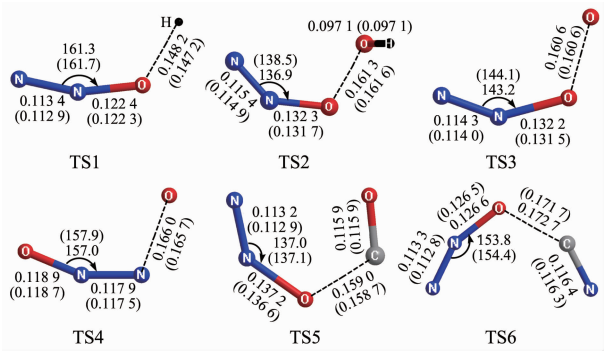

Data in parenthesis belong to the latter, bond length in nm and bond angle in (°)

Fig.2 Structures of transition states at the B3LYP/6-311++G** and B3LYP/aug-cc-pVTZ levels

N_2O is bended by the attacking of other species to form the transition states. On going from the reactants to TS, large bending of N_2O accompanies by a large increment of N-N or N-O bond lengths in the vicinity of attacking species. Of course, the large deformation of N_2O requires large energy compensation in TS2 and TS5 as discussed thereafter.

2.2 Thermodynamic property changes

Table 1 lists the thermodynamic property changes on going from the reactants to TS and to products at 500 K. Discrepancies of the thermodynamic property changes obtained from these two different computational levels are 8.23, 10.04 and 7.17 kJ·mol^{-1} at most for ΔE, ΔH and ΔG, resulting a relative discrepancy of 2% at most. Discrepancy for ΔS is 6.46 J·mol^{-1}. These consistent values indicate that the energetic properties reach their basis set limitation. Discussion for the thermodynamic properties thereafter refers to the data from the aug-cc-pVTZ basis set. The predicted activation energy of ca. 200 kJ·mol^{-1} for reaction (**5**) is in good agreement with the experimental value of (193±8) kJ·mol^{-1} [8]. Kinetically, reaction (**5**) is difficult to occur with an activation free energy ($\Delta G^{\neq}$) of 261 kJ·mol^{-1}, while reaction (**1**) is easy to occur with $\Delta G^{\neq}$ value of 91 kJ·mol^{-1}. Our result is in agreement with the modeling suggestion that the most important N_2O destruction reactions involve the attack of H radical[18]. A quasi-classical trajectory study of H +N_2O also concludes that the direct reaction via O-atom attack dominates[10]. Reaction (**5**) involves two stable reactants and thus is kinetically unfavorable to take place. However, it is thermodynamically favorable to take place with free energy changes (ΔG) of 407 kJ·mol^{-1}. On the contrary, there is an unstable species or radical on the other five reactions. Among these five reactions involving radical reactants, the $\Delta G^{\neq}$ values on going from reactants to TS for reactions (**2**) and (**3**) are much larger since they involves two oxygen-oxygen collision, which is energe-tically unfavorable compared to the

Table 1 Thermodynamic property changes along the reaction paths at 500 K predicted by DFT-B3LYP method[a]

Basis sets	Reaction	Reactants → TS				Reactants → Products			
		$\Delta E^{\neq}$ [b]	$\Delta H^{\neq}$	$\Delta S^{\neq}$	$\Delta G^{\neq}$	ΔE	ΔH	ΔS	ΔG
6-311++G*	(**1**)	51.14	44.57	−93.66	91.40	−259.22	−258.83	26.14	−271.90
	(**2**)	150.24	145.62	−111.23	201.24	−96.97	−97.76	18.95	−107.24
	(**3**)	138.79	134.82	−101.69	185.67	−324.65	−324.05	12.14	−330.12
	(**4**)	75.35	70.55	−104.93	123.02	−149.95	−149.39	23.51	−161.15
	(**5**)	201.24	197.38	−126.02	260.39	−362.76	−363.32	−13.21	−356.71
	(**6**)	55.02	53.02	−109.58	107.81	−417.48	−418.88	−9.26	−414.25
aug-cc-pVTZ	(**1**)	50.87(64)	44.46	−93.10	91.01	−252.56	−251.97	26.89	−265.41
	(**2**)	149.79(42)	145.33	−110.44	200.55	−97.79	−98.39	19.70	−108.24
	(**3**)	136.79(118)	132.92	−101.38	183.61	−327.70	−326.90	12.9	−333.35
	(**4**)	75.10(118)	69.39	−108.52	123.65	−148.08	−147.32	24.28	−159.46
	(**5**)	201.59(184)	197.77	−126.38	260.96	−357.38	−357.76	−6.75	−354.39
	(**6**)	55.39(0)	53.38	−110.93	108.84	−409.25	−408.84	−3.52	−407.08

[a] ΔE, ΔH and ΔG are in kJ·mol^{-1}, ΔS in J·mol^{-1}, ΔE is corrected for the zero-point vibrational energy (ZPE). The scaling factors for the ZPE and thermal correction ($H_{0K\rightarrow TK}$) are 0.96[17]; [b] Data in parenthesis are from ref.[5], the original data in energy units of cal/mol were converted to kJ·mol^{-1} for the convenience of comparison.

collision between electron donor and acceptor as in reaction (**1**). Kilpinen et al. suggested that the OH radical also plays an important role in N_2O destruction [18]. However, there is no evidence to support that suggestion from the DFT calculated data. Reactions (**1**) and (**6**) are kinetically the leading roles in N_2O destruction. At the same time, reaction (**6**) is thermodynamically the easiest process to occur among all the reactions.

Verma et al. solved the nonlinear, first-order differential equations by using the analytical form of the first derivative of the species concentration, in order to calculate the time-dependent composition of various chemical species that evolve from the coal combustion[5]. As shown in Table 1, the activation energies in this work for reaction (**1**) are the largest, while those of reactions (**1**) and (**6**) are the two smallest. At that point, our results are in agreement with Verma′s. However, there is a large disagreement between this work and Verma′s for reaction (**2**). Other disagreements are of reaction (**3**) and (**4**). Though the reactants of (**3**) and (**4**) are identical, there are different TS structures for these two reactions, resulting different activated energies instead of the same ones derived by Verma[5].

Fig.3 and 4 respectively show the enthalpy and entropy changes along the path of reactants to TS at different temperatures from 500 K to 1 800 K. The $\Delta H^{\neq}$ values slightly decrease as temperatures increase for the reactions (**1**), (**3**) and (**4**). However, the $\Delta H^{\neq}$ values hardly change as temperatures increase for reactions (**2**), (**5**) and (**6**). Though the variations of $\Delta H^{\neq}$ values with temperatures are different, the magnitudes of $\Delta H^{\neq}$ values are not crossed, i.e. the $\Delta H^{\neq}$ values of reaction (**1**) are small or much small than all the others. The $\Delta S^{\neq}$ values decrease as temperature increases for the reactions (**1**), (**3**) and (**4**). However, the $\Delta S^{\neq}$ values slightly increase as temperature increases for reactions (**2**), (**5**) and (**6**). There are crossover of $\Delta S^{\neq}$ values around 600 K for reactions (**2**), (**4**) and (**6**). The $\Delta S^{\neq}$ values associate with the collision factors. The collision factor of reaction (4) is larger than those of reactions (**2**) and (**6**) under 600 K. However, the collision factor of reaction (**4**) is much smaller than those of reactions (**2**) and (**6**) when the temperature is much above 600 K.

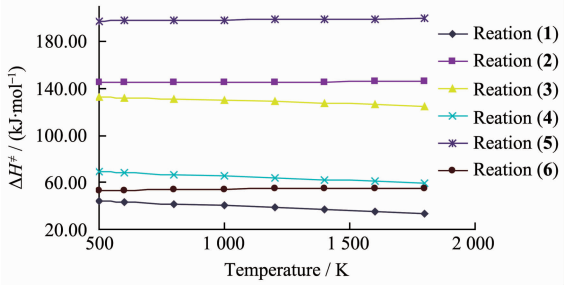

Fig.3　Enthalpy changes along the path of Reactants → TS at different temperatures

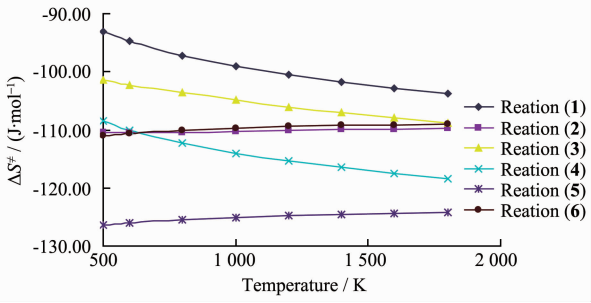

Fig.4　Entropy changes along the path of Reactants → TS at different temperatures

Fig.5 displays the Gibbs free energy changes from reactants to products as temperature varies. The ΔG values for reactions (**1**) through (**4**) slightly decrease as temperature increases, while the ΔG values hardly change with temperature for reactions (**5**) and (**6**). Thermodynamically, reaction (**6**) is much easier to occur than reaction (**2**), since the latter involves a formation of very unstable species of HO_2.

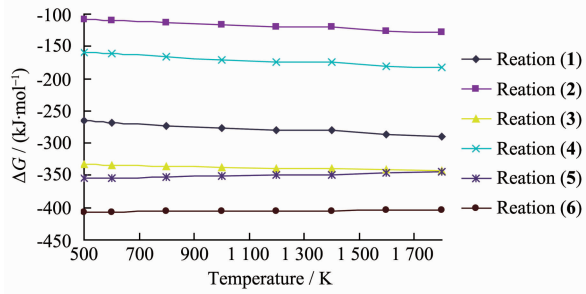

Fig.5　Gibbs free energy changes from reactants to products at different temperatures

2.3　Rate constants

We use transition state theory of Eyring to calculate the rate constants by the following equation:

$$k=\frac{k_B T}{h}\left(\frac{p^{\ominus}}{RT}\right)^{1-n}\exp\left[\frac{\Delta_r^{\neq}S_m^{\ominus}(p^{\ominus})}{R}\right]\exp\left[-\frac{\Delta_r^{\neq}H_m^{\ominus}(p^{\ominus})}{RT}\right]$$

Here, k_B and h are Boltzmann and Plank constants,

respectively; $\Delta_r^{\neq} S_m^{\ominus}$ ($p^{\ominus}$) and $\Delta_r^{\neq} H_m^{\ominus}$ ($p^{\ominus}$) are standard molar entropy and standard molar enthalpy of activation at the condition of $p^{\ominus}$=100 kPa, respectively; n is the sum of computation coefficient for all reactants.

Fig.6 shows the variations of rate constants with temperatures. There are linear relationships between lg(k) and (1/T) for all the reactions. Rate constants of reaction (**5**) increase mostly with temperature increasing compared to all the other reactions. However, there is no crossover among the lines, indicating that the rate constant of reaction (**1**) is the largest while that of reaction (**5**) is the smallest over the temperature range 500~1 800 K. Compared to other reactions, reaction (**5**) involves two stable reactants (N_2O and CO) and thus is kinetically unfavorable to take place.

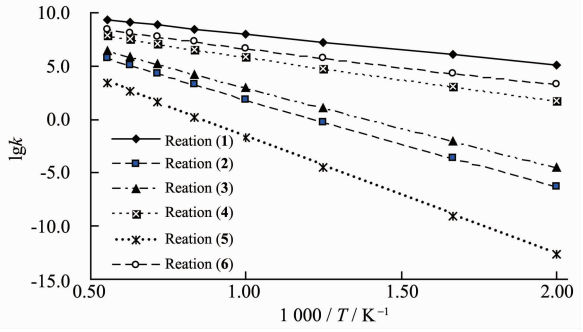

Fig.6 Rate constants at different temperatures

3 Conclusions

Based on the computations for the reactions of N_2O with five species, the following conclusions can be drawn:

(1) Reaction (**1**) is kinetically favorable since it involves a radical reactant as well as a collision between electron donor and acceptor.

(2) Reactions (**1**) and (**6**) are kinetically the leading roles in N_2O destruction. At the same time, reaction (**6**) is thermodynamically the easiest process to occur among all the reactions.

(3) Reaction (**5**) involves two stable reactants and thus is kinetically unfavorable to take place. However, it is thermodynamically favorable to take place.

References:

[1] Weiss R F. *J. Geophys. Res.*, **1981**,**86**:7185-7195

[2] Keller M, Kaplan W A, Wofsy S C. *J. Geophys. Res.*, **1986**,**91**: 11791-11802

[3] Tullin C J, Goel S, Morihara A, et al. *Energy Fuel*, **1993**,**7**: 796-802

[4] Visona S P, Stanmore B R. *Combust. Flame*, **1996**,**106**:207-218

[5] Verma S S, Niwa T, Okazaki K. *Int. J. Energy Res.*, **2001**,**25**: 165-186

[6] Ogawa M, Yoshida N. *Chemosphere*, **2005**,**61**:877-887

[7] Wang Y D, McIlveen-Wright D, Huang Y, et al. *Fuel*, **2007**, **86**:2101-2108

[8] Loirat H, Caralp F, Destriau M, et al. *J. Phys. Chem.*, **1987**,**91**: 6538-6542

[9] Chang K S, Lee H J, Park Y S, et al. *Appl. Catal. A-Gen.*, **2006**,**309**:129-138

[10]Bradley K S, Schatz G C. *J. Phys. Chem.*, **1996**,**100**:12154-12161

[11]WANG Yong-Cheng(王永成), ZHANG Qing-Li(张庆莉), GENG Zhi-Yuan(耿志远), et al. *Acta Chim. Sinica*(*Huaxue Xuebao*), **2008**,**66**:2669-2674

[12]Wang Y C,Wang Q, Geng Z Y, et al. *Chem. Phys. Lett.*, **2010**,**498**:245-252

[13]Becke A D. *J. Chem. Phys.*, **1992**,**96**:2155-2160

[14]Becke A D. *J. Chem. Phys.*, **1993**,**98**:5648-5652

[15]HUANG Yu-Cheng(黄玉成), JU Xue-Hai(居学海), QIU Ling (邱玲), et al. *Chinese J. Inorg. Chem.*(*Wuji Huaxue Xuebao*), **2006**,**22**(11):1962-1966

[16]Frisch M J, Trucks G W, Schlegel H B, et al. *Gaussian* 03, Gaussian, Inc., Pittsburgh, PA, **2003**.

[17]Scott A P, Radom L. *J. Phys. Chem.*, **1996**,**100**(41):16502-16513

[18]Kilpinen P, Hupa M. *Combust. Flame*, **1991**,**85**:94-104